Available online at www.sciencedirect.com
SCIENCE DIRECT®
Journal of Solid State Chemistry 176 (2003) 151–158
JOURNAL OF SOLID STATE CHEMISTRY
http://elsevier.com/locate/jssc

# Phase equilibrium in the system *Ln*–Mn–O VI: *Ln* = Ho and Tb at 1100°C

Kenzo Kitayama,* Minehito Kobayashi, Hisataka Takano, Naomi Nambu, and Hideyuki Hirasawa

*Department of Applied Chemistry and Biotechnology, Faculty of Engineering, Niigata Institute of Technology, Kashiwazaki, Niigata 945-1195, Fujihashi, Japan*

Received 2 April 2003; received in revised form 7 July 2003; accepted 10 July 2003

**Abstract**

Phase equilibria were established in Ho–Mn–O and Tb–Mn–O systems at 1100°C by varying the oxygen partial pressure from $-\log(P_{O_2}/\text{atm}) = 0$–13.00, and phase diagrams for the corresponding $Ln_2O_3$–MnO–$MnO_2$ systems at 1100°C were presented. Stable $Ln_2O_3$, MnO, $Mn_3O_4$, $LnMnO_3$, and $LnMn_2O_5$ phases were found at 1100°C, whereas $Ln_2Mn_2O_7$, $Ln_2MnO_4$, $Mn_2O_3$, and $MnO_2$ were not found to be stable. Small nonstoichiometric ranges were found in the $LnMnO_3$ phase, with the composition of $LnMnO_3$ represented as functions of $\log(P_{O_2}/\text{atm})$, $N_O/N_{HoMnO_3} = 9.0\times10^{-5}(\log P_{O_2})^3 + 1.1\times10^{-3}(\log P_{O_2})^2 + 6.0\times10^{-3}(\log P_{O_2}) + 4.7\times10^{-3}$ and $N_O/N_{TbMnO_3} = 2.00\times10^{-4}(\log P_{O_2})^3 + 3.40\times10^{-3}(\log P_{O_2})^2 + 1.81\times10^{-2}\log P_{O_2} + 3.47\times10^{-2}$. Activities of the components in the solid solution were calculated from these equations. The composition of $LnMnO_3$ may range from $Ln_2O_3$ rich to $Ln_2O_3$ poor, while MnO is slightly nonstoichiometric, being oxygen rich and $LnMn_2O_5$ seems to be nonstoichiometric. Lattice constants of $LnMnO_3$ quenched at different oxygen partial pressures and of $LnMn_2O_5$ quenched in air were determined. The standard Gibbs energy changes of the reactions appearing in the phase diagrams were also calculated. The relationship between the tolerance factor of $LnMnO_3$ and $\Delta G^0$of reaction, $(1/2)Ln_2O_3 + MnO + (1/4)O_2 = LnMnO_3$, is shown graphically.


*Keywords:* Phase equilibrium; Thermogravimetry; Holmium-manganese oxide; Terbium manganese oxide; Gibbs energy

## 1. Introduction

A number of reports deal with the magnetic, electronic, and crystallographic properties of $LaMnO_3$ [1,2]. The magnetic order, moments and ordering temperatures of $La_{1-t}MnO_{3+\delta}$ depend strongly on the nonstoichiometry [3]. Although similar physical properties would be expected in other perovskit-structured lanthanoid-manganese oxides, only a few studies into the phase diagrams that can precisely reveal the nonstoichiometry of $LnMnO_3$ have carried out [4,5].

Recently, phase equilibrium has been established in the *Ln*–Mn–O (*Ln* = La [6], Nd [7], Gd [8], and Sm [9]) systems at 1100°C. According to these studies, there are two types of phase diagrams depending on the number of stable ternary compounds in the *Ln*–Mn–O system, either the single ternary compound $LnMnO_3$ or two ternary compounds, $LnMnO_3$ and $LnMn_2O_5$.

The objectives of the present study are to (1) establish detailed phase diagrams of the Ho–Mn–O and Tb–Mn–O systems at 1100°C as functions of the oxygen partial pressure, (2) identify which type of phase diagram these systems exhibit, (3) measure the lattice constants of ternary compounds, and (4) determine the thermochemical properties based on the phase equilibrium at 1100°C.

## 2. Experimental

Analytical grade $Ho_2O_3$(99.9%) and MnO(99.9%) were used as raw materials.

The MnO was dried by heating in air to 100°C and the $Ho_2O_3$ was dried at 1100°C. $Tb_2O_3$ was prepared from $Tb_4O_7$ (99.9%) at an oxygen partial pressure of $\log P_{O_2} = -9.00$ for 8 h at 1100°C and quenched in the bronze tube attached to the bottom of furnace tube and cooled by ice-water from outside [10,11]. Quenched $Tb_2O_3$ was verified by EDTA titration [11] and powder X-ray diffraction. Mixtures having the desired ratios of

*Corresponding author. Fax: +81-025-722-8142.
*E-mail address:* kitayama@acb.niit.ac.jp (K. Kitayama).

0022-4596/$ - see front matter © 2003 Elsevier Inc. All rights reserved.
doi:10.1016/S0022-4596(03)00380-3

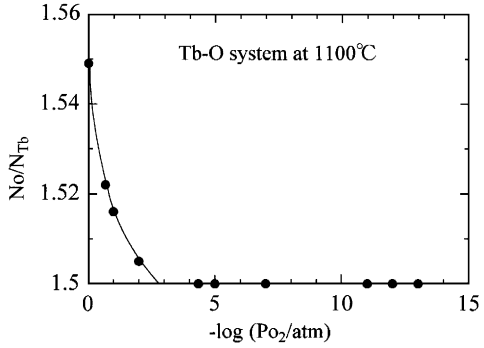


Fig. 1. The relationship between the oxygen partial pressure ($\log(P_{O_2}$/atm) and the O/Tb molar ratio in the Tb–O system.

$Ln_2O_3$/MnO were prepared by mixing thoroughly in an agate mortar and were calcined several times during the intermediate mixing and treated using procedures described previously [12].

The thermogravimetric methods in which oxygen partial pressure was varied by passing a gas or mixture of gases through the furnace were mainly used to establish equilibrium.

Mixed gases of $CO_2$ and $H_2$, and of $CO_2$ and $O_2$ and single-component gas of $O_2$ and $CO_2$ were used to obtain the desired oxygen partial pressures. The apparatus and procedures used to control oxygen partial pressure and to maintain constant temperature, the method of thermogravimetry and the criteria for the establishment of equilibrium have been described previously [12]. To ensure equilibrium, the weight of equilibrium of each sample at a particular oxygen partial pressure was established from both sides of the reaction, i.e., as oxygen partial pressure is increased from a low value and as it is decreased from a high value. The balance, furnace, and gas mixer are schematically shown in Fig. 1 of Ref. [13]. The furnace is composed of a vertically mounted mullite tube wound with Pt 60%–Rh 40% alloy wire as the heating element. The mixed gases that were used to achieve the desired oxygen partial pressure were introduced from the bottom of the furnace and flowed to the top.

The identification of phases and the determination of lattice constants were performed using a Rint 2500 Rigaku X-ray diffractometer, employing Ni-filterd Cu$K\alpha$ radiation. A standard specimen of silicon was used to calibrate $2\theta$ measurements.

## 3. Results and discussions

### 3.1. Phase equilibrium

#### 3.1.1. Mn–O system

The Mn–O system has four known oxides, MnO, $Mn_3O_4$, $Mn_2O_3$, and $MnO_2$. This system was reinvestigated, with the details already reported for the $La_2O_3$–MnO–$MnO_2$ system [6]. Oxygen partial pressure in equilibrium with MnO and $Mn_3O_4$ was found to be $\log(P_{O_2}/\text{atm}) = -5.40 \pm 0.05$ with $Mn_3O_4$ stoichiometric over the range of $-\log(P_{O_2}/\text{atm}) = 0$–5.40. MnO, however, is slightly nonstoichiometric in composition, being oxygen rich with a O/Mn molar ratio of 1.019 at $\log(P_{O_2}/\text{atm}) = -5.40$. The equation of $N_O/N_{MnO} = 9.83 \times 10^{-4} \quad (\log P_{O_2})^2 + 1.914 \times 10^{-2}(\log P_{O_2}) + 0.0933$ was obtained for MnO solid solution over the oxygen partial pressure range from $-10.00$ to $-5.40$ using the least-squares method. Here, $N_O$ and $N_{MnO}$ are the mole fractions of oxygen and MnO in the solid solution.

The oxides MnO and $Mn_3O_4$ were confirmed to be stable, whereas the higher oxides $Mn_2O_3$ and $MnO_2$ were not. This has also been reported by van Roosmalen et al. [14] in the investigation of the pseudobinary $La_2O_3$–$Mn_2O_3$ phase diagram in air (Fig. 6 in Ref. [14]).

#### 3.1.2. Tb–O system

The Tb–O system has been studied at 1000°C, 1100°C, and 1200°C [10,11]. The system was reinvestigated by thermogravimetry at 1100°C, with the resulting relationship between the molar ratio, $N_O/N_{Tb}$, and oxygen partial pressure, $-\log(P_{O_2}/\text{atm})$, shown in Fig. 1. Here, $N_O$ is the mole fraction of oxygen and $N_{Tb}$ is also mole fraction of Tb in Tb-oxide. As can be seen, $Tb_2O_3$ is stable, at least over the range of $-\log(P_{O_2}/\text{atm}) = 13.00$–4.35, but the molar ratio $N_O/N_{Tb}$ then gradually increases to 1.549 ($Tb_2O_{3.098}$ or $Tb_4O_{6.196}$) as the $O_2$ pressure increases to 1 atm. However, the Terbium did not oxidize to $Tb_4O_7$ under the present experimental conditions. Identification of phases in the quenched samples revealed $Tb_2O_3$ phase in the samples examined at all oxygen partial pressures, as shown in Table 1. $Tb_2O_3$ is thus nonstoichiometric with the O-rich $Tb_2O_{3.098}$ under 1 atm $O_2$.

#### 3.1.3. $Ho_2O_3$–MnO–$MnO_2$ system

Six samples having $Ho_2O_3$/MnO molar ratios of 0.6/0.4, 0.4/0.6, 0.3/0.7, 0.25/0.75, 0.15/0.85 and 0.1/0.9 were prepared for thermogravimetric analysis. The relationships between oxygen partial pressure, $-\log(P_{O_2}/\text{atm})$, on the ordinate and the ratio of weight changes, $W_{O_2}/W_T$, on the abscissa are shown for three representative samples of 0.6/0.4, 0.3/0.7, and 0.1/0.9 in Figs. 2(a)–(c), respectively. Here, $W_{O_2}$ is the weight increase of the samples from the reference weight at $\log(P_{O_2}/\text{atm}) = -13.00$, at which $Ho_2O_3$ and MnO are stable, and $W_T$ is the total weight gain from the reference state to the weight at 1 atm $O_2$, at which $Ho_2O_3$ and $HoMnO_3$ or $HoMnO_3$ and $HoMn_2O_5$ or $HoMn_2O_5$ and $Mn_3O_4$ are stable depending on the total composition of the samples. Weight breaks are found at $-\log(P_{O_2}/\text{atm}) = 8.15$, 5.40 and 1.75. These values

Table 1
Identification of phase

| Sample | | $-\log(P_{O_2}/\text{atm})$ | Time (h) | Phases |
|---|---|---|---|---|
| $Ho_2O_3$ | MnO | | | |
| 0.6 | 0.4 | 13.00 | 8 | $Ho_2O_3 + MnO$ |
| | | 8.50 | 21 | $Ho_2O_3 + MnO$ |
| | | 7.00 | 18.5 | $Ho_2O_3 + HoMnO_3$ |
| | | 5.00 | 20.5 | $Ho_2O_3 + HoMnO_3$ |
| | | 0.68 | 23 | $Ho_2O_3 + HoMnO_3$ |
| 0.4 | 0.6 | 13.00 | 8 | $Ho_2O_3 + MnO$ |
| | | 8.50 | 21 | $Ho_2O_3 + MnO$ |
| | | 7.00 | 18.5 | $Ho_2O_3 + HoMnO_3$ |
| | | 5.00 | 20.5 | $Ho_2O_3 + HoMnO_3$ |
| | | 0.68 | 23 | $Ho_2O_3 + HoMnO_3$ |
| 0.25 | 0.75 | 13.00 | 8 | $Ho_2O_3 + MnO$ |
| | | 8.50 | 21 | $Ho_2O_3 + MnO$ |
| | | 7.00 | 18.5 | $HoMnO_3 + MnO$ |
| | | 5.00 | 46.5 | $HoMnO_3 + Mn_3O_4$ |
| | | 0.68 | 89 | $HoMnO_3 + HoMn_2O_5$ |
| 0.1 | 0.9 | 13.00 | 8 | $Ho_2O_3 + MnO$ |
| | | 8.50 | 21 | $Ho_2O_3 + MnO$ |
| | | 7.00 | 18.5 | $HoMnO_3 + MnO$ |
| | | 5.00 | 20.5 | $HoMnO_3 + Mn_3O_4$ |
| | | 0.68 | 89 | $HoMn_2O_5 + Mn_3O_4$ |
| $Tb_2O_3$ | MnO | | | |
| 0.6 | 0.4 | 13.00 | 8 | $Tb_2O_3 + MnO$ |
| | | 9.00 | 23 | $Tb_2O_3 + MnO$ |
| | | 7.00 | 20.5 | $Tb_2O_3 + TbMnO_3$ |
| | | 5.00 | 20 | $Tb_2O_3 + TbMnO_3$ |
| | | 3.00 | 20 | $Tb_2O_3 + TbMnO_3$ |
| | | 0.68 | 96 | $Tb_2O_3 + TbMnO_3$ |
| 0.4 | 0.6 | 13.00 | 8 | $Tb_2O_3 + MnO$ |
| | | 9.00 | 23 | $Tb_2O_3 + MnO$ |
| | | 7.00 | 20.5 | $Tb_2O_3 + TbMnO_3$ |
| | | 5.00 | 20 | $Tb_2O_3 + TbMnO_3$ |
| | | 3.00 | 20 | $Tb_2O_3 + TbMnO_3$ |
| | | 0.68 | 96 | $Tb_2O_3 + TbMnO_3$ |
| 0.25 | 0.75 | 13.00 | 8 | $Tb_2O_3 + MnO$ |
| | | 9.00 | 23 | $Tb_2O_3 + MnO$ |
| | | 7.00 | 20.5 | $MnO + TbMnO_3$ |
| | | 5.00 | 20 | $MnO + TbMnO_3$ |
| | | 3.00 | 20 | $Mn_3O_4 + TbMnO_3$ |
| | | 0.68 | 96 | $TbMn_2O_5 + TbMnO_3$ |
| 0.10 | 0.90 | 13.00 | 8 | $Tb_2O_3 + MnO$ |
| | | 9.00 | 23 | $Tb_2O_3 + MnO$ |
| | | 7.00 | 20.5 | $MnO + TbMnO_3$ |
| | | 5.00 | 20 | $MnO + TbMnO_3$ |
| | | 3.00 | 20 | $Mn_3O_4 + TbMnO_3$ |
| | | 0.68 | 96 | $Mn_3O_4 + TbMn_2O_5$ |
| 1.0 | 0.0 | 9.00 | 7.5 | $Tb_2O_3$ |
| | | 7.00 | 25.5 | $Tb_2O_3$ |
| | | 0.68 | 24 | $Tb_2O_3$ |

correspond to the oxygen partial pressure at which the three solid phases, $Ho_2O_3 + HoMnO_3 + MnO$, $HoMnO_3 + MnO + Mn_3O_4$ and $HoMnO_3 + Mn_3O_4 + HoMn_2O_5$, are in equilibrium. The value $\log P_{O_2} = -5.40$ corresponds to the value at which MnO and $Mn_3O_4$ are in equilibrium, as described above. As can be seen in the figures, the weight gradually changes with oxygen partial pressure due to the presence of solid solutions.

Table 1 shows the results of phase identification in the Ho–Mn–O system. Samples of around 500 mg were prepared for the identification of phases using the quenching method. Five phases, $Ho_2O_3$, MnO, $Mn_3O_4$, $HoMnO_3$, and $HoMn_2O_5$ were found to be stable under the experimental conditions, whereas $Ho_2Mn_2O_7$, $HoMn_2O_4$, $Mn_2O_3$, and $MnO_2$ were not stable.

Based on the results of thermogravimetry and phase identification, a phase diagram was constructed for the $Ho_2O_3$–MnO–$MnO_2$ system, even though $MnO_2$ was not stable under these conditions, as shown in Fig. 3. The numerical values shown in three of solid fields in Fig. 3 are the equilibrium values of $-\log P_{O_2}$ in those solid phases, as described above. Numbers on the lines in the two-phase regions are oxygen partial pressures in $-\log(P_{O_2}/\text{atm})$. Nonstoichiometry of the MnO is ascertained by the results of thermogravimetry of the two samples shown Figs. 2(b) and (c). These represent slight changes in composition over the range of the oxygen partial pressures from $-\log P_{O_2} = \sim 9.00$ to 5, although the weight breaks are found at $\log(P_{O_2}/\text{atm}) = -8.15$ in these figures. As shown in Fig. 3, there are three three-phase regions, $A + B_2 + W_1$, $B_3 + C + W_2$, and $C + D + W_3$ in which the oxygen partial pressures at equilibrium are 8.15, 5.40, and 1.75 in $-\log(P_{O_2}/\text{atm})$, respectively. It must be noticed that there are seven two-phase regions: $Ho_2O_3$–MnO, $Ho_2O_3$–$HoMnO_3$, MnO–$HoMnO_3$, MnO–$Mn_3O_4$, $Mn_3O_4$–$HoMnO_3$, $Mn_3O_4$–$HoMn_2O_5$, and $HoMnO_3$–$HoMn_2O_5$.

$HoMnO_3$ exhibits a slightly small nonstoichiometric composition in the range of $\log P_{O_2} = -8.15$–0. A perovskite-structured $LaMnO_{3+\delta}$ solid solution was reported to be able to be formed with excess La as well as with excess Mn by van Roosmalen et al. [14]. The same phenomenon might be seen in this three-component system. Therefore, the oxygen partial pressure lines in the $HoMnO_3$ phase region may be curved in a way that cannot be represented in the figure. Fig. 4 shows the relationship between the oxygen partial pressure and the ratio $N_O/N_{HoMnO_3}$, as given by the equation $N_O/N_{HoMnO_3} = 9.0 \times 10^{-5} (\log P_{O_2})^3 + 1.1 \times 10^{-3} (\log P_{O_2})^2 + 6.0 \times 10^{-3} (\log P_{O_2}) + 4.7 \times 10^{-3}$. Table 2 lists the compositions, oxygen partial pressures at equilibrium and activities of the components in solid solution using the same symbols as used in Fig. 3.

Lattice constants of the hexagonal $HoMnO_3$ are listed in Table 3. Two samples having $Ho_2O_3$/MnO ratios of 0.4/0.6 and 0.25/0.75 are quenched in two different oxygen partial pressure atmospheres of $-\log P_{O_2} = 7.00$ and 0.68, as well as 5.00 for the latter sample. In the last column of Table 3, other phases that coexist with $HoMnO_3$ are shown. For the $Ho_2O_3$/MnO = 0.4/0.6 sample, $a$, $c$, and $V$ were found to gradually decrease as

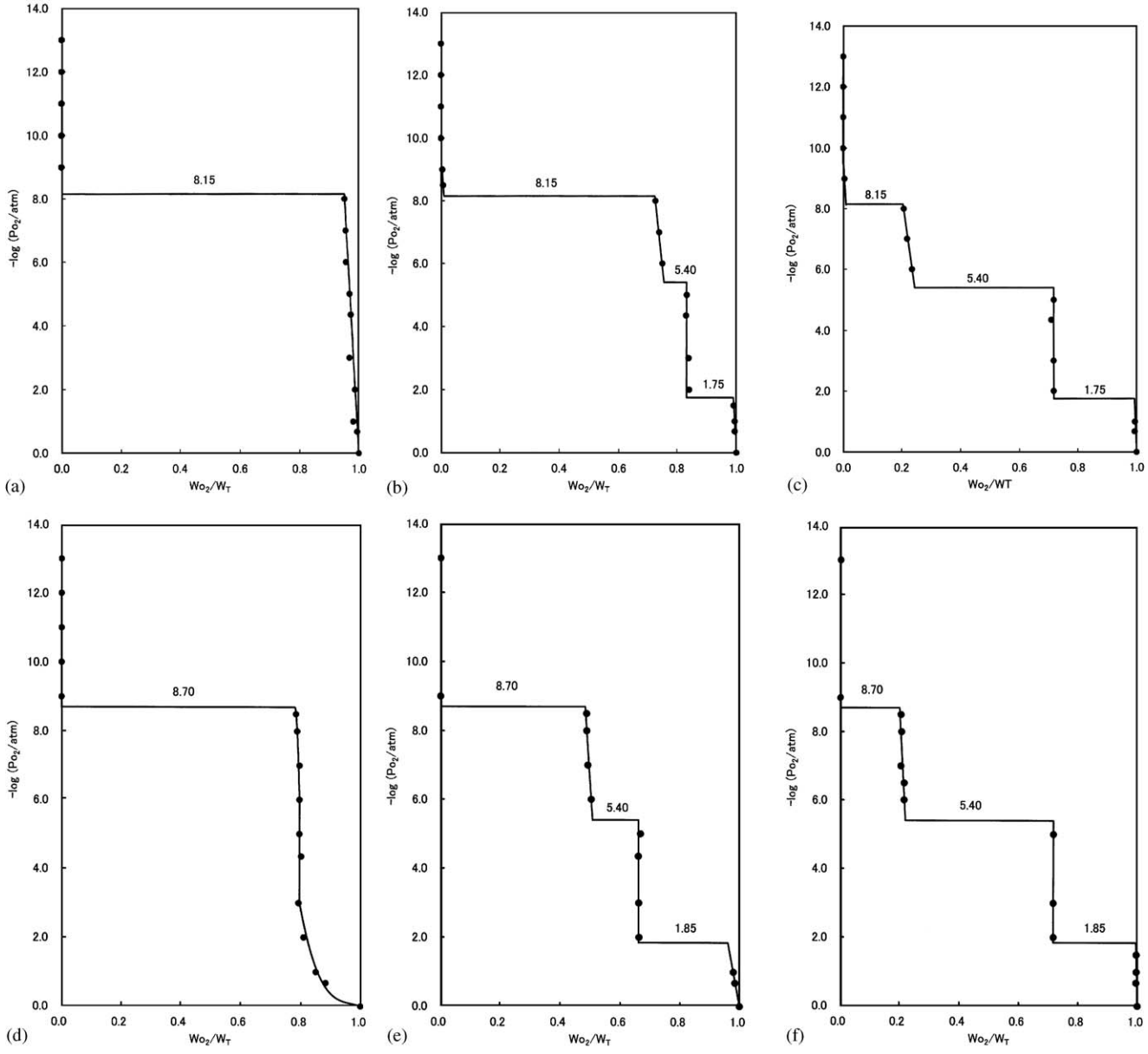


Fig. 2. The relationship between the oxygen partial pressure, $\log(P_{O_2}/\text{atm})$, and the weight change of the samples, $W_{O_2}/W_T$. (a) $Ho_2O_3/MnO = 0.6/0.4$, (b) $Ho_2O_3/MnO = 0.3/0.7$, and (c) $Ho_2O_3/MnO = 0.1/0.9$. (d) $Tb_2O_3/MnO = 0.6/0.4$, (e) $Tb_2O_3/MnO = 0.25/0.75$, and (f) $Tb_2O_3/MnO = 0.1/0.9$.

oxygen partial pressure increased. Although this may be due to an increase in the number of the smaller ionic radius $Mn^{4+}$ ions, the only data available with which to analyze these samples is the higher oxygen partial pressure. For the $Ho_2O_3/MnO = 0.25/0.75$ samples, these values are in good agreement, and the lattice constants are in good agreement with previous values (Ref. [15]).

### 3.1.4. $Tb_2O_3$–MnO–$MnO_2$

Six samples with $Tb_2O_3/MnO$ molar ratios of 0.6/0.4, 0.4/0.6, 0.25/0.75, and 0.1/0.9 were prepared for thermogravimetric analysis. Figs. 2(d)–(f) show the relationships between the oxygen partial pressure, $-\log(P_{O_2}/\text{atm})$, on the ordinate and weight change, $W_{O_2}/W_T$, on the abscissa for three representative samples, 0.6/0.4 (Fig. 2(d)), 0.25/0.75 (Fig. 2(e)), and 0.1/0.9 (Fig. 2(f)). Here, $W_{O_2}$ is the weight increase of the samples from the reference weight at $\log(P_{O_2}/\text{atm}) = -13.00$, at which $Tb_2O_3$ and MnO are stable, and $W_T$ is the total weight gain from the reference state to the weight at 1 atm $O_2$, at which $Tb_2O_3$ and $TbMnO_3$, $TbMnO_3$ and $TbMn_2O_5$, and $TbMn_2O_5$ and $Mn_3O_4$ are stable depending on the total composition of the samples. Weight breaks are found at $-\log(P_{O_2}/\text{atm}) = 8.70$, 5.40, and 1.85. These values correspond to

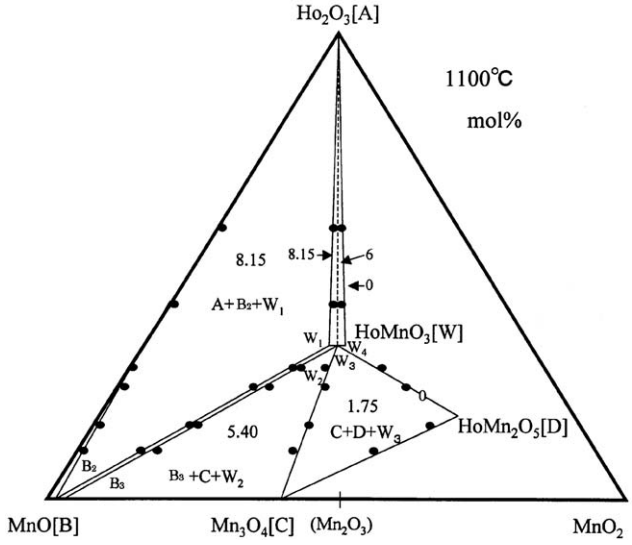


Fig. 3. Phase equilibrium in the $Ho_2O_3$–MnO–$MnO_2$ system at 1100°C. Numerical values indicated in three of the phase regions and on the two-phase lines are oxygen partial pressures in $-\log(P_{O_2}/\text{atm})$ in equilibrium with solid phases shown in each region. Abbreviations are the same as those in Table 2.

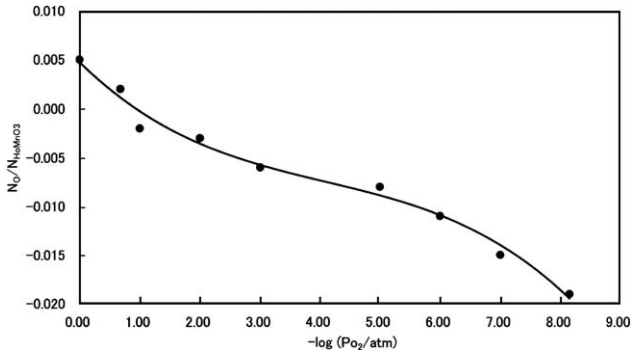


Fig. 4. The relationship between the oxygen partial pressure, $-\log(P_{O_2}/\text{atm})$ and the composition of $HoMnO_3$ solid solution, $N_O/N_{HoMnO_3}$.

Table 2
Compositions, symbols, stability ranges in oxygen partial pressures, and activities of components in solid solutions

| Component | Compositions | Symbols | $-\log(P_{O_2}/\text{atm})$ | $\text{Log}\, a_i$ |
|---|---|---|---|---|
| MnO | $MnO_{1.00}$ | B | 13.00–10.00 | 0 |
| | $MnO_{1.001}$ | $B_1$ | 8.70 | $-4.35\times10^{-4}$ |
| | $MnO_{1.003}$ | $B_2$ | 8.17 | $-7.77\times10^{-4}$ |
| | $MnO_{1.02}$ | $B_3$ | 5.40 | −0.0137 |
| $HoMnO_3$ | $HoMnO_{2.984}$ | $W_1$ | 8.15 | 0 |
| | $HoMnO_{2.992}$ | $W_2$ | 5.40 | 0.0191 |
| | $HoMnO_{2.997}$ | $W_3$ | 1.75 | 0.0313 |
| | $HoMnO_{3.005}$ | $W_4$ | 0.00 | 0.0309 |
| $TbMnO_3$ | $TbMnO_{2.988}$ | $W_5$ | 8.70 | 0 |
| | $TbMnO_{3.002}$ | $W_6$ | 5.40 | $-8.66\times10^{-3}$ |
| | $TbMnO_{3.009}$ | $W_7$ | 1.85 | −0.0185 |
| | $TbMnO_{3.035}$ | $W_8$ | 0.00 | −0.0384 |

the oxygen partial pressure at which the three solid phases, $Tb_2O_3(A)+TbMnO_3(W_5)+MnO(B_1)$, $TbMnO_3(W_1)+MnO(B_3)+Mn_3O_4(C)$, and $TbMnO_3(W_7)+Mn_3O_4(C)+TbMn_2O_5(D)$ are in equilibrium. The partial pressure $\log P_{O_2}=-5.40$ corresponds to equilibrium between MnO and $Mn_3O_4$, as described above.

The results of phase identification of the Tb–Mn–O system are shown in Table 1 with those of the $Ho_2O_3$–MnO–$MnO_2$ system. Five phases, $Tb_2O_3$, MnO, $Mn_3O_4$, $TbMnO_3$, and $TbMn_2O_5$, were found to be stable, whereas $Tb_2Mn_2O_7$, $TbMn_2O_4$, $Mn_2O_3$ and $MnO_2$ were not stable in the present experimental setup.

Based on the above thermogravimetric results and phase identifications, a phase diagram was constructed for the $Tb_2O_3$–MnO–$MnO_2$ system, even though $MnO_2$ is not stable under the experimental conditions, and this is shown in Fig. 5. The numerical values shown in three-phase regions in Fig. 5 are the values of $-\log P_{O_2}$ found for the three solid phases, as described above. Numbers on the lines in the two-phase regions are the oxygen partial pressures in $-\log(P_{O_2}/\text{atm})$. Abbreviations are the same as those in Table 2. It must be noticed that there are seven two-phase regions in Fig. 3.

$TbMnO_3$ is a fairly nonstoichiometric composition in the range of $\log P_{O_2}=-8.70-0$. And $TbMnO_3$ solid solution may have many isobaric lines of oxygen partial pressure. A perovskite-structured $LaMnO_{3+\delta}$ solid solution was reported to be able to be formed with excess La as well as with excess Mn by van Roosmalen et al. [14]. The same phenomenon may also be exhibited by the present system, similar to the Ho–Mn–O system described above. One-phase region has two degrees of freedom in this case, and the oxygen partial pressure lines in the $TbMnO_3$ phase region might thus be curved in a way that could not be represented in the figure.

The relationship between $N_O/N_{TbMnO_3}$ and the oxygen partial pressure for $TbMnO_3$ solid solution is represented by the following equation: $N_O/N_{TbMnO_3}=2.00\times10^{-4}\ (\log P_{O_2})^3+3.40\times10^{-3}\ (\log P_{O_2})^2+1.81\times10^{-2}(\log P_{O_2})+3.47\times10^{-2}$. Here, $N_O$ and $N_{TbMnO_3}$ are the mole fractions of oxygen and $TbMnO_3$ in the solid solution.

Lattice constants of the $TbMnO_3$ are listed in Table 3. Two samples having $Ho_2O_3$/MnO ratios of 0.4/0.6 and 0.25/0.75 are quenched at two different oxygen partial pressures, $-\log P_{O_2}=7.00$ and 0.68. Phases coexisting with $TbMnO_3$ are shown in the last column in Table 3. For the $Tb_2O_3$/MnO = 0.25/0.75 samples, data for $-\log P_{O_2}=5.00$ are also shown. The values are in good agreement, and are reasonable for the narrow range of compositions of $TbMnO_3$ that is found with $Mn_3O_4$ and MnO, as shown in Fig. 5. The lattice constants are also in good agreement with previous values.

Table 3
Lattice constants of quenched $LnMnO_3$

| Sample | | $-\log(P_{O_2}/\text{atm})$ (atm) | $a$ (Å) | $b$ (Å) | $c$ (Å) | $V$ (Å$^3$) | Other phase |
|---|---|---|---|---|---|---|---|
| $Ho_2O_3$ | MnO | | | | | | |
| 0.4 | 0.6 | 7.00 | 6.143(2) | | 11.418(4) | 373.2(2) | $Ho_2O_3$ |
| | | 0.68 | 6.136(2) | | 11.400(5) | 371.7(2) | $Ho_2O_3$ |
| 0.25 | 0.75 | 7.00 | 6.139(2) | | 11.410(4) | 372.5(2) | MnO |
| | | 5.00 | 6.138(1) | | 11.402(3) | 372.1(1) | $Mn_3O_4$ |
| | | 0.68 | 6.140(4) | | 11.398(8) | 372.1(4) | $HoMn_2O_5$ |
| | | | 6.134 | | 11.406 | | Ref. [15] |
| $Tb_2O_3$ | MnO | | | | | | |
| 0.4 | 0.6 | 7.00 | 5.298(1) | 5.843(1) | 7.401(1) | 229.1(1) | $Tb_2O_3$ |
| | | 0.68 | 5.298(2) | 5.842(1) | 7.402(2) | 229.1(1) | $Tb_2O_3$ |
| 0.25 | 0.75 | 7.00 | 5.299(3) | 5.849(3) | 7.396(3) | 229.2(2) | MnO |
| | | 5.00 | 5.302(4) | 5.834(3) | 7.404(4) | 229.0(2) | $Mn_3O_4$ |
| | | 0.68 | 5.312(9) | 5.834(8) | 7.416(8) | 229.8(6) | $TbMn_2O_5$ |
| | | | 5.294 | 5.839 | 7.399 | | Ref. [24] |
| | | | 5.297 | 5.831 | 7.403 | | Ref. [25] |

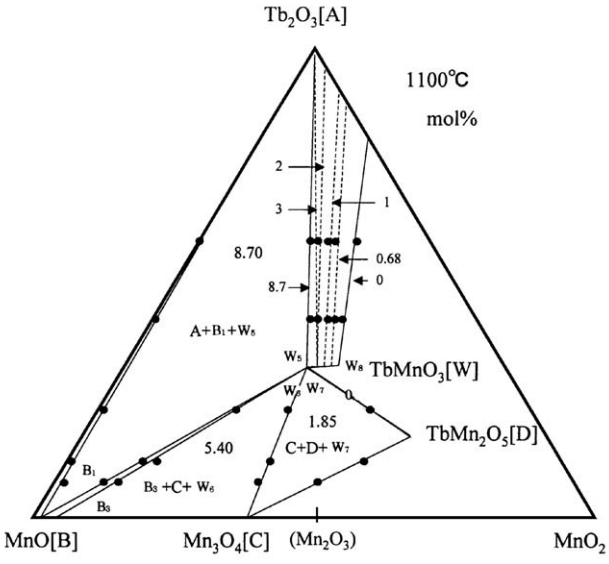


Fig. 5. Phase equilibrium in the $Tb_2O_3$–MnO–$MnO_2$ at 1100°C. Numerical values indicated in three of the phase regions and on the two-phase lines are the oxygen partial pressures in $-\log(P_{O_2}/\text{atm})$ in equilibrium with the solid phases shown in each region. Abbreviations are the same as used in Table 2.

### 3.2. Compound, $LnMn_2O_5$

In the Ho–Mn–O and Tb–Mn–O systems, $LnMn_2O_5$ is stable as a ternary compound, similar to the Gd [8] and Sm [9] systems. It takes more than three days in air to prepare $LnMn_2O_5$ by solid reaction with a mixture of $Ln_2O_3$ and MnO even at 1100°C.

$HoMn_2O_5$ seems to be nonstoichiometric, judging from the slope of Figs. 2(b) and (c) for oxygen partial pressures from $-\log P_{O_2} = 1.75$–0, but this nonstoichiometry is ambiguous in Fig. 3 on account of the scale of the figure. The same nonstoichiometry of $TbMn_2O_5$ was found for oxygen partial pressures of $-\log(P_{O_2}/\text{atm}) = 1.85$–0. Lattice constants of both $HoMn_2O_5$ and $TbMn_2O_5$ were determined based upon $DyMn_2O_5$ data [16], because the ionic radius of Dy is close to that of Ho and Tb. Lattice constant results are shown in Table 4 compared with previously reported values [17,18].

### 3.3. The standard Gibbs energy change of reaction

Based on the phase diagrams established, standard Gibbs energy changes of the reactions listed in Table 5, and in the corresponding phase diagrams, were determined from the equation $\Delta G^0 = -RT\ln K$, where $R$ is the gas constant, $T$ the absolute temperature and $K$ the equilibrium constant of the reaction. The standard state of the activities of components in the solid solutions can be arbitrarily chosen for each solid solution, as indicated by $\log a_i = 0$ in Table 2.

The standard Gibbs energy change for reaction (1) is $-72.1 \pm 0.3$ kJ/mol. Assuming that the activity of MnO of the composition ($B_2$) is unity, this value is $-75.0 \pm 0.3$ kJ/mol, which is not very different due to the small solid solution range, and is in good agreement with the results of Hahn et al. [19]. In addition, the results for reactions [3,5] are in good agreement with those of Satoh et al. [18] even though experimental methods were different.

### 3.4. Relationship between tolerance factor and $\Delta G^0$

The reaction $(1/2)Ln_2O_3 + \text{MnO} + (1/4)O_2 = LnMnO_3$, was found to be common to all of the $Ln$–Mn–O systems studied so far. The relationship between $\Delta G^0$ values of this reaction and tolerance factor ($t$) of perovskite structures having 12-coordinated lanthanoid atoms is shown in Fig. 6. Previous reported values [6–9,22] of $\Delta G^0$ are also shown in Fig. 6 for comparison. The solid

Table 4
Lattice constants of quenched $LnMn_2O_5$

| Sample | | $-\log(P_{O_2}/\text{atm})$ | $a$ (Å) | $b$ (Å) | $c$ (Å) | $V$ (Å)$^3$ | Other phase |
|---|---|---|---|---|---|---|---|
| $Ho_2O_3$ | MnO | | | | | | |
| 0.20 | 0.80 | 0.68 | 7.300(10) | 8.544(9) | 5.676(6) | 354.0(7) | |
| Ref. [17] | | | 7.2643(3) | 8.4768(3) | 5.6700(2) | 349.13(3) | |
| $Tb_2O_3$ | MnO | | | | | | |
| 0.25 | 0.75 | 0.68 | 7.316(3) | 8.527(6) | 5.679(3) | 354.3(4) | $TbMnO_3$ |
| 0.10 | 0.90 | 0.68 | 7.274(5) | 8.567(5) | 5.677(4) | 353.8(4) | $Mn_3O_4$ |
| Ref. [17] | | | 7.3251(2) | 8.5168(2) | 5.6750(2) | 354.04(3) | |
| Ref. [18] | | | 7.278(2) | 8.492(3) | 5.676(2) | 351 | |

Table 5
Standard Gibbs energy changes of reaction at 1100°C

| | Reaction | $-\log(P_{O_2}/\text{atm})$ | $-\Delta G^0$ (kJ/mol) |
|---|---|---|---|
| (1) | $3MnO + (1/2)O_2 = Mn_3O_4$ | $5.40 \pm 0.05$ | $72.1 \pm 0.3$ |
| | | 5.62 | 73.9[a] |
| | | | 60.4[b] |
| | | | 50.9[c] |
| (2) | $(1/2)Ho_2O_3 + MnO + (1/4)O_2 = HoMnO_3$ | $8.15 \pm 0.03$ | $53.6 \pm 0.3$ |
| (3) | $HoMnO_3 + (1/3)Mn_3O_4 + (1/3)O_2 = HoMn_2O_5$ | 1.75 | 14.5 |
| | | 1.79[d] | 14.9 |
| (4) | $(1/2)Tb_2O_3 + MnO + (1/4)O_2 = TbMnO_3$ | 8.70 | 57.2 |
| (5) | $TbMnO_3 + (1/3)Mn_3O_4 + (1/3)O_2 = TbMn_2O_5$ | 1.85 | 16.2 |
| | | 1.87[d] | 16.4 |

[a] Ref. [19].
[b] Ref. [20].
[c] Ref. [21].
[d] Ref. [18].

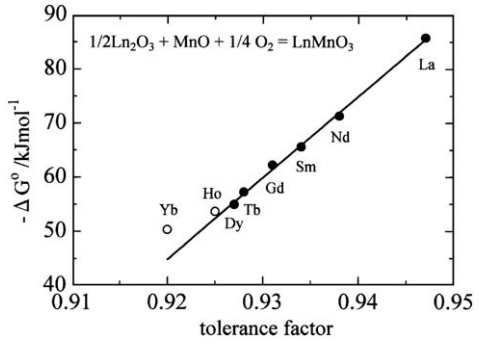


Fig. 6. The relationship between $\Delta G^0$ values of reaction, $(1/2)Ln_2O_3 + MnO + (1/4)O_2 = LnMnO_3$, and the tolerance factor ($t$). Solid circles indicate values of orthorhombic systems, and open circles represent hexagonal systems.

circles represent values of orthorhombic systems and open circles, for hexagonal systems. Ionic radii given by Espinosa [23] were used to calculate the tolerance factors. The crystal structure of $HoMnO_3$ is hexagonal, whereas $TbMnO_3$ is orthorhombic. Thus it may be problematic to adapt tolerance factors based upon the orthorhombic perovskite structure to hexagonal $HoMnO_3$. Ionic radii of $O^{2-}$ and Tb were taken to be 1.40 and 1.292 Å in calculating tolerance factors. A value of 1.281 Å was used for Ho, taken from the value for 12-coordinated garnet, because the ionic radius of 12-coordinated perovskite structures was not found. As can be seen in Fig. 6, the Gibbs energy change of the reaction was nearly proportional to the tolerance factor. The equation $\Delta G^0 = -1.518 \times 10^3 t + 1.352 \times 10^3$ was obtained by fitting to the orthorhombic data. Here, $t$ is the tolerance factor. As shown in Fig. 6, the value for Ho appear to deviate from the line fitting the other lanthanoid perovskite values. This would possibly be due to the differences in the crystal structures as well as Yb.

### 3.5. Conclusion

(1) Phase equilibria in the system $Ln$–Mn–O ($Ln$ = Ho and Tb) at 1100°C were established under an oxygen partial pressure from 0 to −13.00 in $\log(P_{O_2}/\text{atm})$.
(2) Under the present experimental conditions, the $Ln_2O_3$, MnO, $Mn_3O_4$, $LnMnO_3$ and $LnMn_2O_5$ phases are stable.
(3) MnO, $LnMnO_3$, and $LnMn_2O_5$ have non-stoichiometric composition. However, $Mn_3O_4$ is

stoichiometric. The nonstoichiometry of $LnMn_2O_5$ could not be shown in Figs. 3 and 5 due to the scale of figures.

(4) Lattice constants of $LnMnO_3$ and $LnMn_2O_5$ were determined and compared with their previous values.

(5) Standard Gibbs energies of reactions found in the diagram were calculated with the oxygen partial pressure in equilibrium with three solid phases.

(6) $\Delta G^0$ values for the reaction $(1/2)Ln_2O_3 + MnO + (1/4)O_2 = LnMnO_3$, is nearly proportional to the tolerance factor of the perovskite structure. But $\Delta G^0$ values for the hexagonal $LnMnO_3$ deviate from the $\Delta G^0$ vs. $t$ line for the orthorhombic $LnMnO_3$.

## References

[1] J.B. Goodenough, Prog. Solid State Chem. 5 (1971) 149.
[2] C.N.R. Rao, Annu. Rev. Phys. Chem. 40 (1989) 291.
[3] B.C. Hauback, H. Fjellvag, N. Sakai, J. Solid State Chem. 124 (1996) 43.
[4] V.A. Cherepanov, L.Yu. Barkhatova, A.N. Petrov, V.I. Voronin, J. Solid State Chem. 118 (1995) 53.
[5] N. Kamegashira, Y. Miyazaki, Mater. Res. Bull. 19 (1984) 1201.
[6] K. Kitayama, J. Solid State Chem. 153 (2000) 336.
[7] K. Kitayama, T. Kanzaki, J. Solid State Chem. 158 (2001) 236.
[8] K. Kitayama, H. Ohno, R. Ide, K. Satoh, S. Murakami, J. Solid State Chem. 166 (2002) 285.
[9] K. Kitayama, M. Kobayashi, T. Kimoto, J. Solid State Chem. 167 (2002) 160.
[10] T. Sugihara, Thesis, Tokyo Institute of Technology, 1978.
[11] K. Kitayama, J. Solid State Chem. 77 (1988) 366.
[12] K. Kitayama, K. Nojiri, T. Sugihara, T. Katsura, J. Solid State Chem. 56 (1985) 1.
[13] K. Kitayama, J. Solid State Chem. 137 (1998) 255.
[14] J.A.M. van Roosmalen, P. van Vlaanderen, E.H.P. Cordfunke, W.L. Ijdo, D.J.W. Ijdo, J. Solid State Chem. 114 (1995) 516.
[15] JCPDS Card No. 25-1059.
[16] JCPDS Card No. 72-1696.
[17] J.A. Alonso, M.T. Casais, M.J. Martinez-Lope, J.L. Martinez, M.T. Fernandez-Diaz, J. Phys: Condens. Matter 9 (1997) 8515.
[18] H. Satoh, S. Suzuki, K. Yamamoto, N. Kamegashira, J. Alloys Compd. 234 (1996) 35.
[19] W.C. Hahn Jr., A. Muan, Am. J. Sci. 258 (1960) 66.
[20] R.A. Robie, et al., Geol. Survey Bull. 1452 (1978) 1452.
[21] J.F. Elliott, M. Gleiser, in: Thermochemistry for Steelmaking, Vol. 1, Addison-Wesley, Reading, MA, 1960.
[22] K. Kitayama, H. Ohno, M. Kurahashi, E. Koizumi, M. Inagaki, J. Solid State Chem., in Press.
[23] G.P. Espinosa, J. Chem. Phys. 37 (1962) 2344.
[24] JCPDS Card No. 25-0933.
[25] JCPDS Card No. 72-0379.